Preprints of the 19th World Congress
The International Federation of Automatic Control
Cape Town, South Africa. August 24-29, 2014

Distributed parameter modeling of flexible ball screws using Ritz series discretization

B. Henke * **O. Sawodny** * **R. Neumann** **

* *Institute for System Dynamics, University of Stuttgart, Pfaffenwaldring 9, 70569 Stuttgart, Germany*
** *Festo AG & Co. KG, Ruiter Straße 82, 73734 Esslingen, Germany*

Abstract: Ball screw drives are used in automation applications and machine tools to translate rotational motion of an electric motor into translational motion of a slide. Their frequency responses show characteristic torsional and translational resonances. The resonance frequencies vary with the slide position, which is due to the distributed stiffness and inertia of the flexible ball screw. The proposed model treats the ball screw as a flexible element, using Ritz series expansions to obtain a finite approximation of the continuous deformations. The model shows excellent validation results and reproduces the variation of the resonance frequencies with high accuracy.

Keywords: ball screw drive, mechanical systems, distributed-parameter systems, modelling

1. INTRODUCTION

Linear motion in automation systems is mostly generated by mechanically translating the rotational motion of an electric motor into a linear, translational motion of a slide. Ball screw drives are one frequently used mechanism for this translation of rotational to linear motion.

Fig. 1 shows a schematic drawing of a ball screw drive. The motor is connected via an elastic coupling to the ball screw, which is supported by two rotational bearings. The rotational motion of the motor translates into a linear, translational motion of the nut, moving along the ball screw shaft. The slide mounted on the nut carries the load or workpiece and is usually supported by a linear guideway (not depicted in the image).

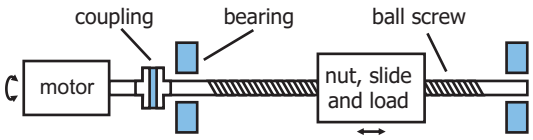

Fig. 1. Schematic drawing of a ball screw drive

Ball screw drives are available in various sizes, ranging from a few centimeters of ball screw length up to several meters. They are used for moving workpieces in industrial automation and handling, as feed drives in machine tools or as lead screws in milling machines. The focus of this paper is on ball screw drives for industrial automation, most commonly in the range of 30 cm to 2 m ball screw length.

Experiments with industrial scale ball screw drives show translational and torsional resonances of the ball screw shaft. The observed resonance frequencies are dependent on the load mass that is mounted on the slide and also on the current position of the slide along the ball screw shaft. The resonance frequencies move to lower frequencies as the slide moves from the motor to the far end of the ball screw. The position dependence can be explained by the distributed stiffness and inertia of the ball screw shaft and motivates the derivation of a distributed parameter model.

Lateral bending oscillations may be relevant for very long and slender ball screws, but are found to be non-dominant for the considered ball screw drives. This is in accordance with the literature on ball screw drives that focuses on the modeling of translational and rotational motion.

Models of ball screw drives differ especially in their treatment of the ball screw itself. They separate into models treating the ball screw shaft as one or multiple rigid bodies and distributed parameter models treating the ball screw shaft as a flexible element. The latter use various approaches to discretize the distributed parameter models. The following paragraphs give a short overview of current modeling approaches.

Pislaru et al. [2004] separate the ball screw shaft into four rigid segments, three for rotation and one for translation, that are connected by springs and dampers. Validation of the model against a measured frequency response shows good quantitative fit of the first two resonances. However, no variation of the load mass or slide position is considered. Frey et al. [2012] present a model that uses two rigid segments each for the rotational and translational motion of the ball screw drive. They account for the position dependence of the resonance frequencies by introducing a position-dependent axial stiffness of the ball screw. Unfortunately, the model for the coupling of rotation and translation and the resulting system equations are not presented in the paper. The model shows good validation results for frequency responses with two different load masses and slide positions.

Varanasi and Nayfeh [2004] use a wave equation and assume quasi-stationary behavior to derive a discretized model with two degrees of freedom. Due to the low order of the discretization, the model can represent only one resonance in the frequency response. No variation of the load mass or slide position is considered. Whalley et al. [2005] use a distributed parameter model in the frequency domain, coupled to rigid bodies modeling the slide and the motor and nonlinearities such as backlash and friction. The resulting model is validated against step responses.

Holroyd et al. [2003] and Zaeh et al. [2004] present finite element models of the ball screw with good validation results in the frequency domain. Again no variation of the load mass or slide position is considered.

When modeling ball screw drives, validation against frequency responses for different operating conditions is very important. The model has to provide exact results for a wide range of possible load masses and slide positions. Given the high number of parameters used in these models, there is be a considerable risk of over-fitting the parameters to one specific operating condition if only one validation experiment is performed.

A promising model approach was presented recently by Vicente et al. [2012]. They characterize the dynamics of the continuous flexible ball screw shaft in terms of kinetic and potential energy. A Ritz series expansion is then used to obtain a finite discrete approximation. The derivation of the system equations is explained in more detail in Vicente et al. [2009].

This paper extends the ideas of Vicente et al. [2012] using a problem specific discretization, allowing for a lower order of the discretized model and yielding superior validation results. The validation also covers various load masses and slide positions along the ball screw.

The rest of this paper is organized as follows: In Sec. 2 a model for the ball screw drive is derived. The system dynamics are characterized in terms of kinetic and potential energy, modeling the ball screw as a flexible shaft with distributed parameters while the motor and the slide are modeled as rigid bodies connected to the ball screw by concentrated elasticities. A Ritz series expansion is then applied to obtain a finite approximation of the distributed parameter energy expressions. The equations of motion are derived by means of Lagrange equations. In Sec. 3 the model is extended by dissipative terms accounting for structural damping of the ball screw shaft. The model is validated in Sec. 4 against frequency responses for different load masses and slide positions. Finally, Sec. 5 gives a short conclusion of the results.

2. MODEL OF THE FLEXIBLE BALL SCREW DRIVE

The ball screw drive considered here is sketched in Fig. 1. The motor is connected to the ball screw by an elastic coupling. The ball screw itself is supported by two bearings, of which the one close to the motor is a thrust bearing allowing only for rotational motion of the ball screw shaft, whereas the one at the free end allows for axial and rotational motion. This avoids stress in the ball screw caused by temperature deformation. The thrust bearing is modeled as a linear elastic connection with high stiffness. The nut connects the slide to the screw and translates the rotational motion of the screw into a translational motion of the slide. The screw-nut interface is considered to be a linear elastic connection. Finally, a rigid load mass is mounted onto the slide.

The model accounts for rotational and translational motion of the ball screw drive. The rotational motion consists of the rotation of the motor as well as the rotation and torsion of the ball screw shaft. The translational motion includes the axial translation and deformation of the ball screw shaft and the translation of slide and load. The rotational and translational motion are assumed to be mutually independent and only coupled by the screw-nut interface.

This model approach considers the ball screw shaft as a flexible element with distributed elasticity and inertia. The motor, slide and load are modeled as rigid bodies, connected to the flexible ball screw by concentrated linear elastic interfaces. Fig. 2 shows the mechanical model with the rotational and translational degrees of freedom characterized by the axial translation $u(x,t)$ and the rotation $\theta(x,t)$ of the ball screw shaft, the motor rotation $\theta_\mathrm{m}(t)$ and the translation of the slide $u_s(t)$. Positions along the flexible screw are defined by the variable x, with $x = 0$ being the position of the motor-side end of the ball screw, $x = L$ the free end of the (undeformed) ball screw and $x = x_s$ the position of the slide. Spring and damper pairs depict the concentrated linear elastic connections of coupling and bearing at $x = 0$ and the screw-nut interface at $x = x_s$.

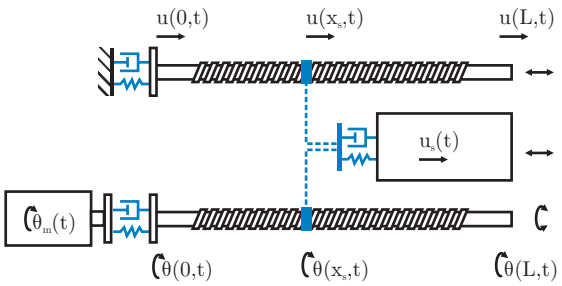

Fig. 2. Mechanical model of the ball screw drive with rotational and translational degrees of freedom.

2.1 Formulation of energy expressions

Variational methods in analytical mechanics, especially the application of Lagrange equations, allow to derive the equations of motion from expressions of the potential and kinetic energy of the overall system.

The potential energy of the flexible ball screw shaft, subject to torsion and axial deformation, can be written as (Reddy [2002])

$$V_\mathrm{s} = \int_0^L \frac{GI}{2}\left[\frac{\partial\,\theta(x,t)}{\partial x}\right]^2 dx + \int_0^L \frac{EA}{2}\left[\frac{\partial\,u(x,t)}{\partial x}\right]^2 dx \tag{1}$$

with the shear modulus G, the area moment of inertia I, Young's modulus E and the (constant) cross section area A of the ball screw shaft.

The kinetic energy regarding the distributed torsion and deformation of the ball screw shaft is

$$T_\mathrm{s} = \int_0^L \frac{\rho I}{2} \left[\frac{\partial\, \theta(x,t)}{\partial t}\right]^2 dx + \int_0^L \frac{\rho A}{2} \left[\frac{\partial\, u(x,t)}{\partial t}\right]^2 dx \tag{2}$$

with the mass density ρ of the ball screw shaft.

Including the concentrated elasticities in the energy expression results in the overall potential energy

$$\begin{aligned} V = &\frac{1}{2} k_\mathrm{b} \left[u(0,t)\right]^2 + \frac{1}{2} k_\mathrm{c} \left[\theta_\mathrm{m}(t) - \theta(0,t)\right]^2 \\ &+ \frac{1}{2} k_\mathrm{n} \left[u_\mathrm{s}(t) - u(x_\mathrm{s},t) - \gamma\theta(x_\mathrm{s},t)\right]^2 \\ &+ \int_0^L \frac{GI}{2} \left[\frac{\partial\, \theta(x,t)}{\partial x}\right]^2 dx + \int_0^L \frac{EA}{2} \left[\frac{\partial\, u(x,t)}{\partial x}\right]^2 dx \end{aligned} \tag{3}$$

with the stiffness of the bearing k_b, the coupling k_c and the screw-nut interface k_n. The second line of this equation characterizes the elastic coupling between the translation of the slide and the rotation and translation of the ball screw shaft. The transmission ratio of the ball screw mechanism γ is the ratio of translational motion of the nut to shaft rotation.

Similarly, including the concentrated masses yields the overall kinetic energy

$$\begin{aligned} T = &\frac{1}{2} \left(m_\mathrm{s} + m_\mathrm{l}\right) \left[\frac{\partial\, u_\mathrm{s}(t)}{\partial t}\right]^2 \\ &+ \frac{1}{2} \left(J_\mathrm{m} + \frac{J_\mathrm{c}}{2}\right) \left[\frac{\partial\, \theta_\mathrm{m}(t)}{\partial t}\right]^2 + \frac{1}{2}\frac{J_\mathrm{c}}{2} \left[\frac{\partial\, \theta(0,t)}{\partial t}\right]^2 \\ &+ \int_0^L \frac{\rho I}{2} \left[\frac{\partial\, \theta(x,t)}{\partial t}\right]^2 dx + \int_0^L \frac{\rho A}{2} \left[\frac{\partial\, u(x,t)}{\partial t}\right]^2 dx \end{aligned} \tag{4}$$

with the masses m_s of the slide and m_l of the load and the moments of inertia J_m of the motor and J_c of the coupling. The latter is split in equal parts to both sides of the elastic coupling.

2.2 Ritz-series expansion

In order to obtain a finite approximation of the continuous deformation of the ball screw shaft, the method of Ritz-series expansion (Reddy [2002]) is applied. This method, proposed by the swiss mathematician Walter Ritz, seeks to approximate the continuous deformation $u(x,t)$ by a finite series expansion of the form

$$u(x,t) = \sum_{i=1}^{N_u} \psi_{u,i}(x) q_{u,i}(t) = \boldsymbol{\psi}_u^T(x) \boldsymbol{q}_u(t) \tag{5}$$

with the basis functions $\boldsymbol{\psi}_u(x) \in \mathbb{R}^{N_u}$ and the coordinates $\boldsymbol{q}_u(t) \in \mathbb{R}^{N_u}$. The basis functions $\boldsymbol{\psi}_u(x)$ are a linear independent and complete set of continuous functions, that need to satisfy the essential boundary conditions of the system. An increasing number N_u of basis functions will improve the accuracy of the approximation.

Similarly, the continuous rotation and torsion of the ball screw shaft is approximated by the finite series expansion

$$\theta(x,t) = \sum_{i=1}^{N_\theta} \psi_{\theta,i}(x) q_{\theta,i}(t) = \boldsymbol{\psi}_\theta^T(x) \boldsymbol{q}_\theta(t) \tag{6}$$

with the basis functions $\boldsymbol{\psi}_\theta(x) \in \mathbb{R}^{N_\theta}$ and the coordinates $\boldsymbol{q}_\theta(t) \in \mathbb{R}^{N_\theta}$.

Inserting the Ritz series expansions (5) and (6) to the expressions for the potential and kinetic energy (3) and (4) results in the following finite approximation

$$\begin{aligned} V = &\frac{1}{2} k_\mathrm{b} \boldsymbol{q}_u^T \boldsymbol{\psi}_u(0) \boldsymbol{\psi}_u(0)^T \boldsymbol{q}_u + \frac{1}{2} k_\mathrm{c} \left[\theta_\mathrm{m} - \boldsymbol{\psi}_\theta^T(0) \boldsymbol{q}_\theta\right]^2 \\ &+ \frac{1}{2} k_\mathrm{n} \left[u_\mathrm{s} - \boldsymbol{\psi}_u^T(x_\mathrm{s}) \boldsymbol{q}_u - \gamma \boldsymbol{\psi}_\theta(x_\mathrm{s}) \boldsymbol{q}_\theta\right]^2 \\ &+ \frac{GI}{2} \boldsymbol{q}_\theta^T \int_0^L \left[\frac{\partial\, \boldsymbol{\psi}_\theta(x)}{\partial x}\right] \left[\frac{\partial\, \boldsymbol{\psi}_\theta(x)}{\partial x}\right]^T dx\, \boldsymbol{q}_\theta \\ &+ \frac{EA}{2} \boldsymbol{q}_u^T \int_0^L \left[\frac{\partial\, \boldsymbol{\psi}_u(x)}{\partial x}\right] \left[\frac{\partial\, \boldsymbol{\psi}_u(x)}{\partial x}\right]^T dx\, \boldsymbol{q}_u \end{aligned} \tag{7}$$

and

$$\begin{aligned} T = &\frac{1}{2} \left(m_\mathrm{s} + m_\mathrm{l}\right) \dot{u}_\mathrm{s}^2 + \frac{1}{2} \left(J_\mathrm{m} + \frac{J_\mathrm{c}}{2}\right) \dot{\theta}_\mathrm{m}^2 \\ &+ \frac{1}{2}\frac{J_\mathrm{c}}{2} \dot{\boldsymbol{q}}_\theta^T \boldsymbol{\psi}_\theta(0) \boldsymbol{\psi}_\theta^T(0) \dot{\boldsymbol{q}}_\theta \\ &+ \frac{\rho I}{2} \dot{\boldsymbol{q}}_\theta^T \int_0^L \boldsymbol{\psi}_\theta(x) \boldsymbol{\psi}_\theta(x)^T dx\, \dot{\boldsymbol{q}}_\theta \\ &+ \frac{\rho A}{2} \dot{\boldsymbol{q}}_u^T \int_0^L \boldsymbol{\psi}_u(x) \boldsymbol{\psi}_u(x)^T dx\, \dot{\boldsymbol{q}}_u \end{aligned} \tag{8}$$

using the common dot-notation for the time derivative of the coordinates.

Various choices are possible for the basis functions $\boldsymbol{\psi}_u$ and $\boldsymbol{\psi}_\theta$. Common choices are sinusoidal functions of increasing frequency or polynomial functions of increasing order. An efficient, problem specific choice of the basis functions allows for lower approximation orders N_u and N_θ. For the flexible ball screw shaft, a good approximation of the first two modes can be achieved with a low order approximation of $N_u = N_\theta = 2$. The basis functions

$$\psi_{u,1}(x) = 1 \quad \text{for } x \in [0, L], \tag{9a}$$

$$\psi_{u,2}(x) = \begin{cases} \frac{x}{x_\mathrm{s}} & \text{for } x \in [0, x_\mathrm{s}] \\ 1 & \text{for } x \in (x_\mathrm{s}, L] \end{cases} \tag{9b}$$

and

$$\psi_{\theta,1}(x) = 1 \quad \text{for } x \in [0, L], \tag{10a}$$

$$\psi_{\theta,2}(x) = \begin{cases} \frac{x}{x_\mathrm{s}} & \text{for } x \in [0, x_\mathrm{s}] \\ 1 & \text{for } x \in (x_\mathrm{s}, L] \end{cases} \tag{10b}$$

account for the known structure of the ball screw drive and treat only the first part of the ball screw shaft as flexible, neglecting deformations of the load-free end of the ball screw.

2.3 Equations of motion

Evaluating the integral terms in (7) and (8) for this choice of the basis functions $\boldsymbol{\psi}_u$ and $\boldsymbol{\psi}_\theta$ and collecting the coordinates in a vector

$$\boldsymbol{q} = \begin{bmatrix}\theta_\mathrm{m} & u_\mathrm{s} & \boldsymbol{q}_\theta^T & \boldsymbol{q}_u^T\end{bmatrix}^T \in \mathbb{R}^{N_u+N_\theta+2} \tag{11}$$

results in the matrix expression for the kinetic and potential energy

$$T = \frac{1}{2} \dot{\boldsymbol{q}}^T \boldsymbol{M} \dot{\boldsymbol{q}}, \tag{12}$$

$$V = \frac{1}{2} \boldsymbol{q}^T \boldsymbol{K} \boldsymbol{q}. \tag{13}$$

The mass matrix $\boldsymbol{M}$ has block-diagonal structure and can be written as

$$\boldsymbol{M} = \begin{bmatrix} J_\mathrm{m} + \frac{J_\mathrm{c}}{2} & 0 & 0 & 0 & 0 & 0 \\ 0 & m_\mathrm{s} + m_\mathrm{l} & 0 & 0 & 0 & 0 \\ 0 & 0 & \rho I L + \frac{J_\mathrm{c}}{2} & \rho I\, \tilde{l}(\frac{1}{2}) & 0 & 0 \\ 0 & 0 & \rho I\, \tilde{l}(\frac{1}{2}) & \rho I\, \tilde{l}(\frac{2}{3}) & 0 & 0 \\ 0 & 0 & 0 & 0 & \rho A L & \rho A\, \tilde{l}(\frac{1}{2}) \\ 0 & 0 & 0 & 0 & \rho A\, \tilde{l}(\frac{1}{2}) & \rho A\, \tilde{l}(\frac{2}{3}) \end{bmatrix}$$

using the abbreviation $\tilde{l}(\alpha) = L - \alpha x_\mathrm{s}$. The stiffness matrix

$$\boldsymbol{K} = \begin{bmatrix} k_\mathrm{c} & 0 & -k_\mathrm{c} & 0 & 0 & 0 \\ 0 & k_\mathrm{n} & -\gamma\, k_\mathrm{n} & -\gamma\, k_\mathrm{n} & -k_\mathrm{n} & -k_\mathrm{n} \\ -k_\mathrm{c} & -\gamma\, k_\mathrm{n} & \gamma^2\, k_\mathrm{n} + k_\mathrm{c} & \gamma^2\, k_\mathrm{n} & \gamma\, k_\mathrm{n} & \gamma\, k_\mathrm{n} \\ 0 & -\gamma\, k_\mathrm{n} & \gamma^2\, k_\mathrm{n} & \frac{GI}{x_\mathrm{s}} + \gamma^2\, k_\mathrm{n} & \gamma\, k_\mathrm{n} & \gamma\, k_\mathrm{n} \\ 0 & -k_\mathrm{n} & \gamma\, k_\mathrm{n} & \gamma\, k_\mathrm{n} & k_\mathrm{n} + k_\mathrm{b} & k_\mathrm{n} \\ 0 & -k_\mathrm{n} & \gamma\, k_\mathrm{n} & \gamma\, k_\mathrm{n} & k_\mathrm{n} & \frac{AE}{x_\mathrm{s}} + k_\mathrm{n} \end{bmatrix}$$

is highly coupled due to the elastic screw-nut interface modeled with stiffness k_n.

To obtain the equations of motion for the ball screw drive, the Lagrange equations

$$\frac{d}{dt}\left(\frac{\partial\, L}{\partial \dot{\boldsymbol{q}}}\right) - \frac{\partial\, L}{\partial \boldsymbol{q}} = \boldsymbol{f} \tag{14}$$

are evaluated for the Lagrange function $L = T - V$ with the kinetic energy T and the potential energy V according to (12) and (13). This yields the equations of motion

$$\boldsymbol{M}\ddot{\boldsymbol{q}} + \boldsymbol{K}\boldsymbol{q} = \boldsymbol{f} \tag{15}$$

with

$$\boldsymbol{f} = [\tau_\mathrm{m}\ 0\ 0\ 0\ 0\ 0]^T \tag{16}$$

representing the motor torque.

3. DISSIPATION MODEL

The model derived so far is a non-dissipative model, neglecting the structural damping of the ball screw and the damping of the discrete elasticities of coupling, bearing and nut. These damping effects are now included in the model using a dissipation function $R(\dot{\boldsymbol{q}})$, as introduced by Rayleigh [1877]. The dissipation function characterizes the energy dissipated by viscous damping, i.e. of damping forces proportional to the relative velocities in the system. It extends the common representation of the Lagrange equations (14) to

$$\frac{d}{dt}\left(\frac{\partial\, L}{\partial \dot{\boldsymbol{q}}}\right) - \frac{\partial\, L}{\partial \boldsymbol{q}} = -\frac{\partial\, R}{\partial \dot{\boldsymbol{q}}} + \boldsymbol{f}. \tag{17}$$

The dissipation function for the structural damping of the ball screw shaft can be written as

$$R_\mathrm{s} = \int_0^L \frac{\eta G I}{2}\left[\frac{\partial\, \dot{\theta}(x,t)}{\partial x}\right]^2 dx + \int_0^L \frac{\eta E A}{2}\left[\frac{\partial\, \dot{u}(x,t)}{\partial x}\right]^2 dx \tag{18}$$

assuming the damping coefficient to be proportional to the stiffness by a factor η.

Including the damping of the concentrated elasticities results in the overall dissipation function

$$\begin{aligned} R = {} & \frac{1}{2} d_\mathrm{b} \left[\dot{u}(0,t)\right]^2 + \frac{1}{2} d_\mathrm{c} \left[\dot{\theta}_\mathrm{m}(t) - \dot{\theta}(0,t)\right]^2 \\ & + \frac{1}{2} d_\mathrm{n} \left[\dot{u}_\mathrm{s}(t) - \dot{u}(x_\mathrm{s},t) - \gamma \dot{\theta}(x_\mathrm{s},t)\right]^2 \\ & + \int_0^L \frac{\eta G I}{2}\left[\frac{\partial\, \dot{\theta}(x,t)}{\partial x}\right]^2 dx \\ & + \int_0^L \frac{\eta E A}{2}\left[\frac{\partial\, \dot{u}(x,t)}{\partial x}\right]^2 dx \end{aligned} \tag{19}$$

with the damping coefficients of the bearing d_b, the coupling d_c and the screw-nut interface d_n.

Applying the Ritz series expansion (5) and (6) yields the following finite approximation

$$\begin{aligned} R = {} & \frac{1}{2} d_\mathrm{b} \dot{\boldsymbol{q}}_u^T \boldsymbol{\psi}_u(0) \boldsymbol{\psi}_u(0)^T \dot{\boldsymbol{q}}_u + \frac{1}{2} d_\mathrm{c} \left[\dot{\theta}_\mathrm{m} - \boldsymbol{\psi}_\theta^T(0) \dot{\boldsymbol{q}}_\theta\right]^2 \\ & + \frac{1}{2} d_\mathrm{n} \left[\dot{u}_\mathrm{s} - \boldsymbol{\psi}_u^T(x_\mathrm{s}) \dot{\boldsymbol{q}}_u - \gamma \boldsymbol{\psi}_\theta(x_\mathrm{s}) \dot{\boldsymbol{q}}_\theta\right]^2 \\ & + \frac{\eta G I}{2} \dot{\boldsymbol{q}}_\theta^T \int_0^L \left[\frac{\partial\, \boldsymbol{\psi}_\theta(x)}{\partial x}\right]\left[\frac{\partial\, \boldsymbol{\psi}_\theta(x)}{\partial x}\right]^T dx\, \dot{\boldsymbol{q}}_\theta \\ & + \frac{\eta E A}{2} \dot{\boldsymbol{q}}_u^T \int_0^L \left[\frac{\partial\, \boldsymbol{\psi}_u(x)}{\partial x}\right]\left[\frac{\partial\, \boldsymbol{\psi}_u(x)}{\partial x}\right]^T dx\, \dot{\boldsymbol{q}}_u. \end{aligned} \tag{20}$$

This can be evaluated for the basis functions (9) and (10), resulting in the matrix representation

$$R = \frac{1}{2} \dot{\boldsymbol{q}}^T \boldsymbol{D} \dot{\boldsymbol{q}} \tag{21}$$

with $\boldsymbol{q}$ as defined in (11) and the damping matrix

$$\boldsymbol{D} = \begin{bmatrix} d_\mathrm{c} & 0 & -d_\mathrm{c} & 0 & 0 & 0 \\ 0 & d_\mathrm{n} & -\gamma\, d_\mathrm{n} & -\gamma\, d_\mathrm{n} & -d_\mathrm{n} & -d_\mathrm{n} \\ -d_\mathrm{c} & -\gamma\, d_\mathrm{n} & \gamma^2\, d_\mathrm{n} + d_\mathrm{c} & \gamma^2\, d_\mathrm{n} & \gamma\, d_\mathrm{n} & \gamma\, d_\mathrm{n} \\ 0 & -\gamma\, d_\mathrm{n} & \gamma^2\, d_\mathrm{n} & \frac{\eta GI}{x_\mathrm{s}} + \gamma^2\, d_\mathrm{n} & \gamma\, d_\mathrm{n} & \gamma\, d_\mathrm{n} \\ 0 & -d_\mathrm{n} & \gamma\, d_\mathrm{n} & \gamma\, d_\mathrm{n} & d_\mathrm{n} + d_\mathrm{b} & d_\mathrm{n} \\ 0 & -d_\mathrm{n} & \gamma\, d_\mathrm{n} & \gamma\, d_\mathrm{n} & d_\mathrm{n} & \frac{\eta AE}{x_\mathrm{s}} + d_\mathrm{n} \end{bmatrix}$$

Evaluating the Lagrange equations (17) for the dissipation function (21) and the kinetic and potential energy according to (12) and (13) yields the equations of motion

$$\boldsymbol{M}\ddot{\boldsymbol{q}} + \boldsymbol{D}\dot{\boldsymbol{q}} + \boldsymbol{K}\boldsymbol{q} = \boldsymbol{f} \tag{22}$$

with the input vector $\boldsymbol{f}$ as specified in (16).

4. EXPERIMENTAL VALIDATION

The experimental validation is based on frequency response data. The data was recorded on a commercially available industrial ball screw drive with a 1500 W motor and a ball screw of 900 mm length and 22 mm diameter.

All frequency response plots in this chapter show frequency responses from the motor current, which is proportional to the generated torque τ_m, to the motor angular velocity θ_m. The velocity signal is obtained from high resolution encoder measurements by numerically differentiating and low pass filtering the position signal. Alterations of the frequency response due to amplifier delay and low pass filtering are compensated for in the frequency domain. Therefore, model and measurements show only the mechanical frequency response of the ball screw drive.

While most of the model parameters are known geometric or material parameters, some need to be identified. These are especially the stiffness parameters k_c, k_b, k_n and damping coefficients d_c, d_b, d_n and η. Fig. 3 shows the magnitude and phase of the frequency response with an additional load of $m_l = 60\,\text{kg}$ and the slide positioned in the middle of the ball screw, i.e. at $x_s = 0.45\,\text{m}$. The model with fitted parameters is in great accordance with the measured data. Especially the two dominant resonance frequencies at 68 Hz and 366 Hz are matched exactly in shape and frequency. The deviation at very low frequencies is due to unmodeled friction effects.

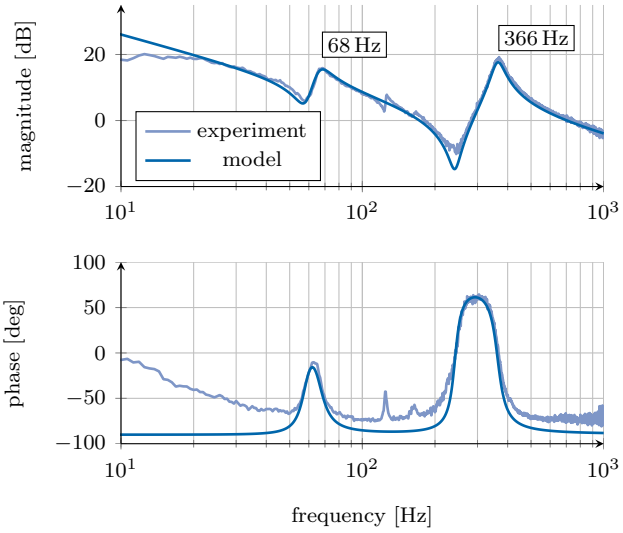

Fig. 3. Frequency response of the ball screw drive with an additional load of 60 kg and the slide in the middle of the ball screw.

Modal analysis (Janschek [2012]) of the system equations (15) reveals that the first mode at 68 Hz is predominantly translational vibration whereas the second mode is predominantly torsional vibration of the ball screw drive. This is in accordance with results for similar setups obtained by FEM simulation (Zaeh et al. [2004]) or modal analysis (Vicente et al. [2012]).

In the following, the high accuracy of the model is validated for different load masses and slide positions. Frequency response data was recorded with four different loads of 30 kg, 60 kg, 90 kg and 120 kg and three different slide positions: close to the motor ($x_s = 0.05\,\text{m}$), in the middle of the ball screw ($x_s = 0.45\,\text{m}$) and far from the motor ($x_s = 0.85\,\text{m}$).

Fig. 4 shows the magnitude of frequency responses for varying loads of $m_l = 90\,\text{kg}$ and $m_l = 120\,\text{kg}$ with the slide in the middle position $x_s = 0.45\,\text{m}$. Compared to Fig. 3, the first (i.e. translational) resonance moves to lower frequencies as the mass increases. This is well reflected by the model that still shows a great fit of the measurements. Note that only the parameter m_l for the load mass is adjusted, while all other model parameters remain unchanged.

In Fig. 5, frequency responses are evaluated for two different positions of the slide, close and far from the motor, with a load of $m_l = 30\,\text{kg}$. Both resonance frequencies are

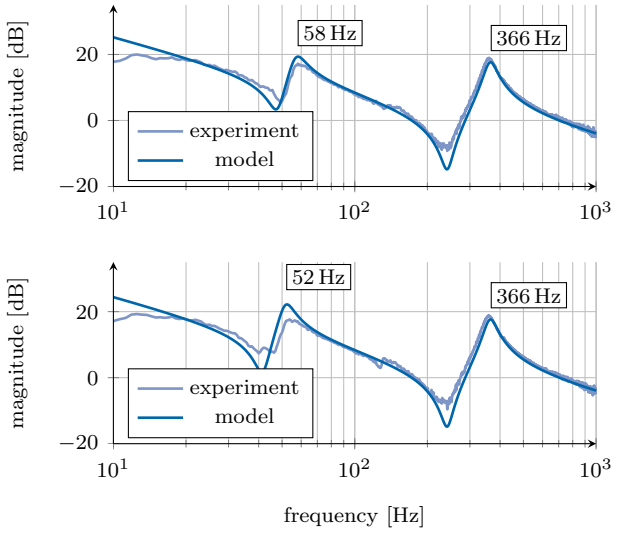

Fig. 4. Frequency response with different loads: 90 kg (top) and 120 kg (bottom) and the slide in the middle of the ball screw.

influenced by the change of the slide position and move to lower frequencies as the slide moves further away from the motor. This dependence on the slide position is caused by the distributed elasticity and inertia of the flexible ball screw shaft and confirms the distributed parameter approach of the model.

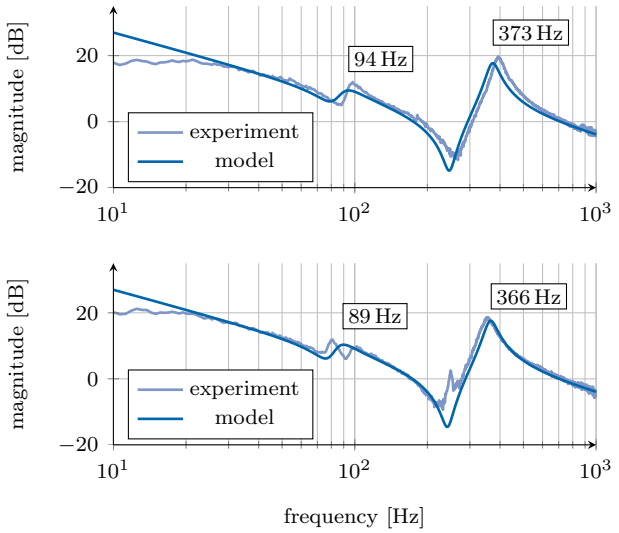

Fig. 5. Frequency response with an additional load of 30 kg for different positions of the slide: close to the motor(top) and far from the motor (bottom).

The dependence of the resonance frequencies on varying load mass and slide positions is summarized in Fig. 6. The frequency of the first and second resonance, as predicted by the model, are plotted against the slide position. This reveals an apparently linear dependence of the first resonance frequency on the slide position and a strong influence of the load mass. The measured frequency responses shown in Fig. 3 to Fig. 5 are marked with blue squares. With the marks being very close to the frequencies predicted by the model, this again proves the high accuracy of the model for a wide range of loads and

slide positions. The maximum measured deviation of the predicted frequencies is 2.5 % for a load of $m_l = 120\,\mathrm{kg}$ and the slide at $x_s = 0.45\,\mathrm{m}$ (Fig. 4). For the second resonance, the load mass has no influence at all and the dependence on the slide position is evidently nonlinear. Here the maximum deviation is 4.2 %, found for a load of $m_l = 30\,\mathrm{kg}$ and the slide at $x_s = 0.05\,\mathrm{m}$ (Fig. 5).

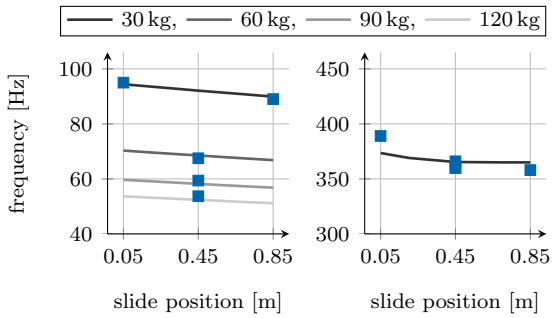

Fig. 6. First and second resonance frequencies for different load masses and slide positions as predicted by the model. The measured frequency responses shown in Fig. 3 to Fig. 5 are marked by blue squares.

5. CONCLUSION

The proposed model for ball screw drives treats the ball screw shaft as a flexible element with distributed parameters and uses Ritz series expansions to obtain a finite approximation of the continuous deformations. Discretizing the model using problem-specific basis functions yields a good approximation of the first two modes with a total of six degrees of freedom for the overall system of ball screw, motor and slide.

Validation against measured frequency responses yields excellent results for various different operating conditions. The dependence of the resonance frequencies on varying load masses and slide positions is reproduced by the model with high accuracy.

REFERENCES

S. Frey, A. Dadalau, and A. Verl. Expedient modeling of ball screw feed drives. *Production Engineering Research Development*, 6:205–211, 2012.

G. Holroyd, C. Pislaru, and D. G. Ford. Modelling the dynamic behaviour of a ball-screw system taking into account the changing position of the ball-screw nut. In *Laser Metrology and Machine Performance VI.*, pages 337–347. WIT Press, Southampton, 2003.

K. Janschek. *Mechatronic systems design: methods, models, concepts.* Springer, 2012.

C. Pislaru, D. G. Ford, and G. Holroyd. Hybrid modelling and simulation of a computer numerical control machine tool feed drive. *Proceedings of the Institution of Mechanical Engineers, Part I: Journal of Systems and Control Engineering*, 218(2):111–120, 2004.

J. W. S. Rayleigh. *The Theory of Sound.* Macmillan, London, 1877.

J. N. Reddy. *Energy principles and variational methods in applied mechanics.* Wiley New York, 2002.

K. K. Varanasi and S. A. Nayfeh. The dynamics of lead-screw drives: low-order modeling and experiments. *ASME Journal of dynamic systems, measurement and control*, 126(2):388–396, 2004.

D. A. Vicente, R. L. Hecker, and G. M. Flores. Ball screw drive systems: evaluation of axial and torsional deformations. In *Mecánica Computacional Vol XXVIII*, 2009.

D. A. Vicente, R. L. Hecker, F. J. Villegas, and G. M. Flores. Modeling and vibration mode analysis of a ball screw drive. *International Journal of Advanced Manufacturing Technology*, 58:257–265, 2012.

R. Whalley, M. Ebrahimi, and A. A. Abdul-Ameer. Hybrid modelling of machine tool axis drives. *International Journal of Machine Tools and Manufacture*, 45(14): 1560–1576, 2005.

M. F. Zaeh, T. Oertli, and J. Milberg. Finite element modelling of ball screw feed drive systems. *CIRP Annals – Manufacturing Technology*, 53(1):289–292, 2004.